

BY RICHARD E. RUSSO  
LAWRENCE BERKELEY NATIONAL LABORATORY  
BERKELEY, CALIFORNIA 94720

# Laser Ablation

## INTRODUCTION

“**L**aser ablation” conjures up star-wars images of a high-powered laser beam obliterating anything in its path! In reality, this view is accurate. When a short-pulsed, high-peak-power laser beam is focused onto any solid target, a portion of the material instantaneously explodes into vapor. The drawing in Fig. 1 is a conceptual interpretation of laser ablation. Photographs in Figs. 2 and 3 show target results after laser ablation (with the use of multiple pulses and different laser-beam energies). Laser “craters” resemble those caused by meteorites striking a planet or volcanic eruptions.

This paper briefly describes laser ablation as it is used with analytical spectroscopy for chemical analysis. I apologize for not citing numerous excellent papers related to the studies presented herein; however, this paper is not a review, but rather serves as an introduction to the field. The name “laser ablation” is used generically to describe the explosive *laser–material interaction*, a more appropriate definition that does not imply a mechanism. “Laser sampling” will refer to the removal of material from a solid with the use of a pulsed laser beam with vapor transport to an analytical excitation source for analysis. Laser sampling has been coupled with practically every analytical source, with the most prevalent today being the inductively coupled plasma (ICP).<sup>1–6</sup>

Laser–material interactions involve coupling of optical energy into

a solid, resulting in vaporization; ejection of atoms, ions, molecular species, and fragments; shock waves; plasma initiation and expansion; and a hybrid of these and other processes. Many models have been developed to describe these processes, but each pertains only to a separate component of the interaction and is applicable only under limited conditions. There are no models that completely describe explosive laser ablation processes (unless the star-wars or fusion-energy folks have worked out such models—and they are classified). Laser irradiance (power density) and the thermo-optical properties of the material are critical parameters that influence these processes. Two general descriptions for the laser–material interaction are described on the basis of irradiance: *vaporization* and *ablation*.<sup>7–12</sup>

**Vaporization.** When the laser pulse duration is microseconds or

longer and the irradiance is less than approximately  $10^6 \text{ W/cm}^2$ , vaporization is likely a dominant process influencing material removal from a target. Phonon relaxation rates are on the order of 0.1 ps, and absorbed optical energy is rapidly converted into heat. Heat dissipation and vaporization are fast in comparison to the laser pulse duration. The thermal and optical properties of the sample influence the amount of material removed during the laser pulse. The optical properties (absorption and reflection) determine both the fraction of the incident power that is absorbed and the depth of optical absorption within the sample. Different heating and cooling rates are expected if the depth of absorption is greater or less than the thermal diffusion length in the material. Although this interaction is defined as vaporization, the energy is delivered in a very short time and it is localized; thermodynamic models do not complete-

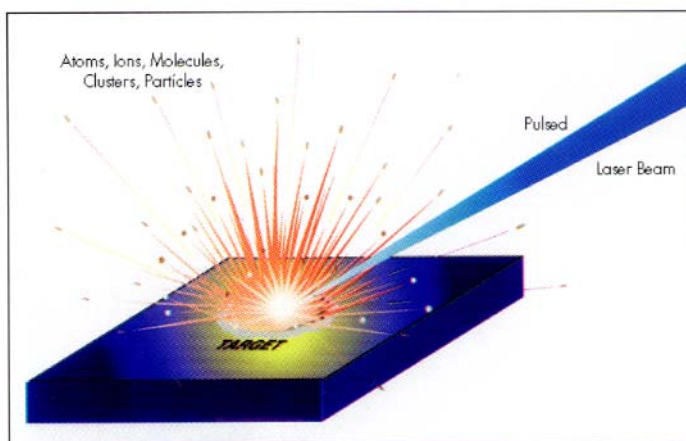


FIG. 1. Conceptual drawing of laser ablation.

ly describe the interaction. Also, optical and thermal properties of the material vary during the laser pulse, which makes it difficult to accurately predict the amount of energy coupled to the target and the quantity of mass removed. However, the interaction is predominantly thermal. Melting is common and fractional vaporization is possible; elements of higher vapor pressure will be enriched in the vapor relative to their concentration in the solid. Amazingly, this vaporization laser–material interaction is considered the easier case! When the irradiance is higher, the interaction is more complicated.

**Ablation.** At higher irradiance, beyond  $10^9$  W/cm<sup>2</sup> with nanosecond and shorter laser pulses focused onto any material, an *explosion* occurs. The term “laser ablation” has been adopted to describe this interaction; it must sound better than “laser explosion”. Phenomenologically, the surface temperature is *instantaneously* heated past its vaporization temperature through linear one-photon absorption, multi-photon absorption, dielectric breakdown, and additional undefined mechanisms.<sup>8,9,11</sup> The vaporization temperature of the surface is exceeded within a fraction of the laser pulse duration; energy dissipation through vaporization from the surface is slow relative to the laser pulse width. Before the surface layer can vaporize, underlying material will reach its vaporization temperature. Temperature and pressure of the underlying material are raised beyond their critical values, causing the surface to explode. The pressure over the irradiated surface from the recoil of vaporized material can be as high as  $10^5$  MPa ( $10^6$  atmospheres).<sup>13</sup> This explosive interaction has been described as “non-thermal”, and melting is often not observed around the crater. Fractional vaporization should be negligible! However, during an ablative interaction, a plasma is initiated at the sample. Plasma temperatures are in excess of  $10^4$  K, and radiative heat transport can establish a *plasma–material* interaction.<sup>8,9,14</sup> The plasma duration is microseconds, which is long

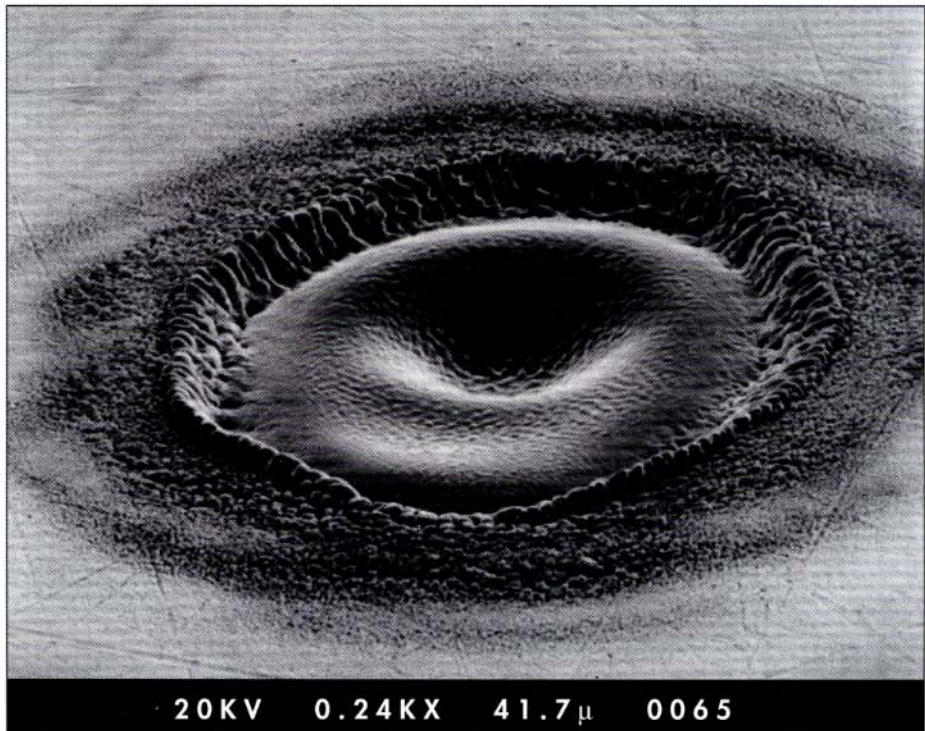


FIG. 2. Photograph of laser ablation “crater” in copper surface with the use of 30-ps pulses from a Nd:YAG laser at  $\lambda = 1064$  nm.

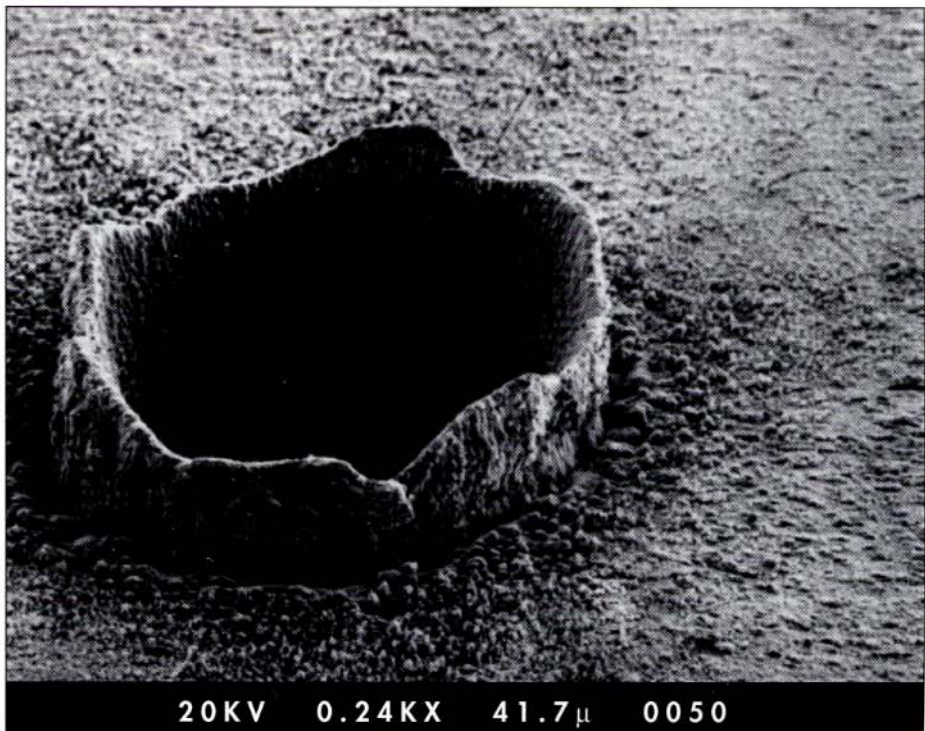
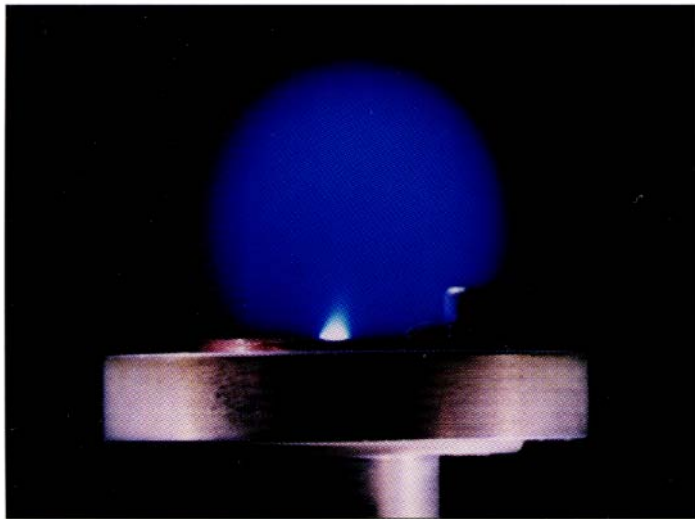


FIG. 3. Photograph of laser ablation “crater” in copper surface with the use of 30-ps pulses from a Nd:YAG laser at  $\lambda = 266$  nm.



**FIG. 4.** Photograph of laser-induced plasma during laser ablation of copper with the use of the nanosecond excimer laser ( $\lambda = 248 \text{ nm}$ ) at a power density of  $3 \times 10^9 \text{ W/cm}^2$ . Gas environment was 100 mTorr of oxygen.

in comparison to the short laser pulse. Fractional vaporization may occur during this plasma–material interaction, and to a greater extent than is the case in the direct laser vaporization interaction. A photograph of a laser-induced plasma (LIP) during UV nanosecond laser ablation of copper is shown in Fig. 4. The luminous laser-induced surface plasma is evident, with cooler spectral emission at the outer parts of the expanding plasma. As an example of how easy it is to achieve high power densities for laser ablation, a 10-ns laser pulse with only 1 mJ of energy, focused to a 10- $\mu\text{m}$  spot size\*(radius), has fluence equal to  $300 \text{ J/cm}^2$  and irradiance of approximately  $4 \times 10^{10} \text{ W/cm}^2$ !

The classification of these mechanisms is simplified and phenomenological; the power densities given for vaporization and ablation are

merely approximate. Power densities in the  $10^6$ – $10^9 \text{ W/cm}^2$  range can cause vaporization, ablation, both of these processes simultaneously, or additional mechanisms that have not yet been identified. One should view these examples as ideal cases; ejection of solid fragments and ions, condensation of clusters, and shock waves occur. Table I lists some of the mechanisms that have been studied. The existence of shock waves is easily confirmed by the sonic boom heard by anyone who has witnessed a focused short-pulse laser exploding target materials at atmospheric pressure.

#### LASER ABLATION AND ATOMIC EMISSION SPECTROSCOPY

Laser ablation is an excellent technology for directly vaporizing solid

samples for elemental analysis by the ICP with the use of either atomic emission spectroscopy (AES) or mass spectrometry (MS) detection. In turn, analytical atomic emission spectroscopy is an excellent technology for studying laser ablation mechanisms. AES can provide fundamental information on the laser plasma such as electron density, temperature, and temporal properties. By transporting the sampled vapor to a separate analytical atomization/excitation source (the ICP is emphasized in this work), one can exploit additional capabilities of AES for studying laser ablation mechanisms. If the ICP conditions are constant, changes in the interaction due to laser parameters, inert gas environment, and material properties can be studied by observing elemental emission intensity in the ICP, temporally and spatially. ICP-AES is probably the best technology for studying laser ablation at atmospheric pressure. AES is emphasized over mass spectrometry (ICP-MS) in order to eliminate issues related to vacuum sampling from the atmospheric-pressure ICP. However, ICP-MS would provide increased sensitivity for studying trace constituent behavior and fundamental properties such as the ablation threshold. Chemical analysis benefits from laser ablation sampling and laser ablation benefits from analytical atomic emission spectroscopy for studying fundamental mechanisms. The remainder of this paper describes some symbiotic relationships.

**Laser Ablation Sampling for Analytical Spectroscopy.** A generalized experimental system for laser sampling and analysis by ICP-AES is shown in Fig. 5. The beam from a pulsed laser is directed into the “ablation” chamber and focused onto the sample (target) surface. Samples are usually placed before the effective focus of the lens to eliminate breakdown and plasma formation directly within the gas. The ablated-sample vapor is carried by the gas flow to the central channel of the ICP torch. Dual gas-inlet ports allow mixing of gases in the ICP for fundamental studies. Spectral emis-

**TABLE I.** Laser ablation mechanisms.

- Absorption (single, multiphoton, defect initiated, ...)
- Reflection (time-dependent)
- Thermodynamics (melting, latency, phase change, ...)
- Plasma ignition
- Shock waves (gas)
- Stress waves (solid)
- Laser–plasma interaction (inverse bremsstrahlung, ...)
- Plasma radiation/heating
- Gas-dynamic expansion
- Hydrodynamic expansion
- ????

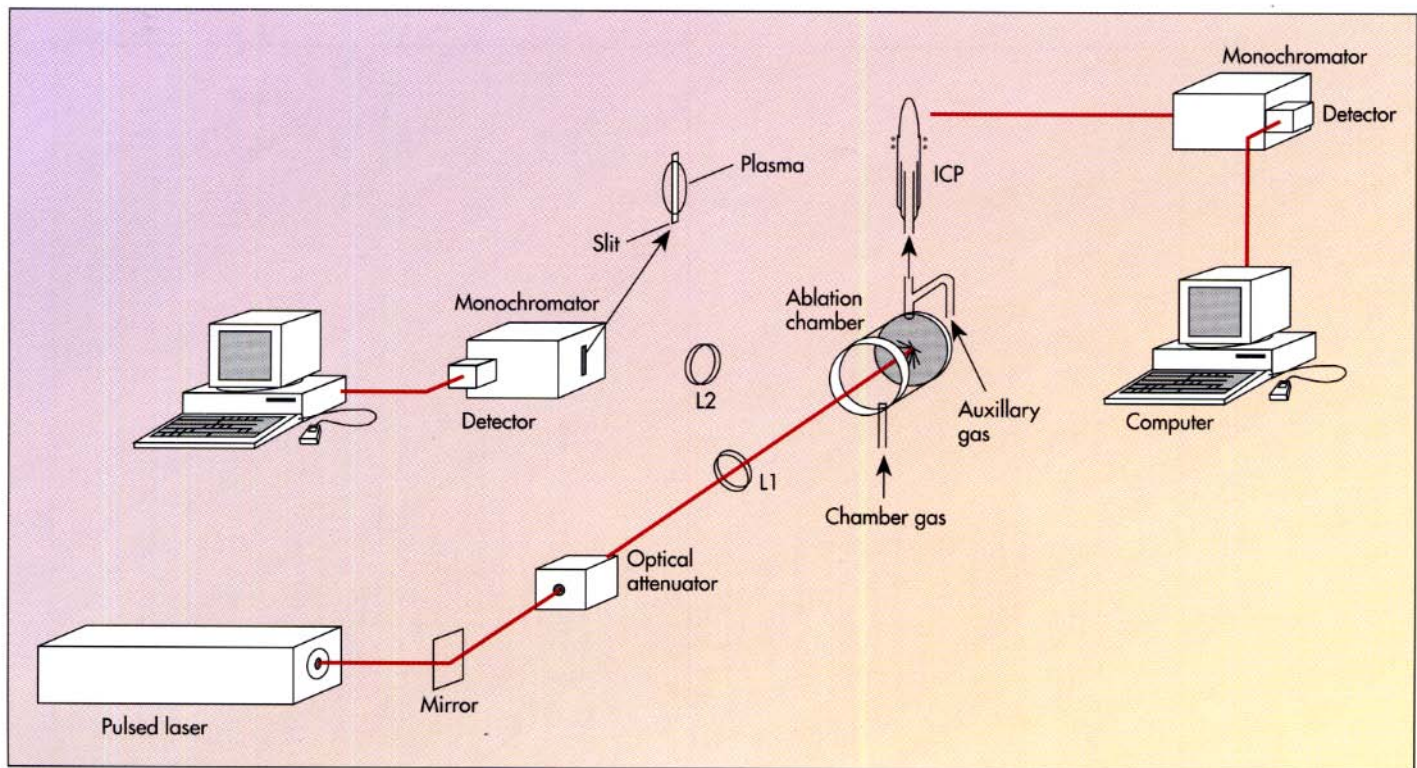


**FIG. 5. General experimental diagram for laser ablation, with the use of inductively coupled plasma atomic emission spectroscopy and laser-induced plasma atomic emission spectroscopy.**

sion from the ICP is measured by a monochromator with several detectors including a photomultiplier tube (PMT), photodiode array (PDA), and charged-coupled device (CCD). If the ablation chamber is constructed of quartz, emission from the laser-induced plasma can be imaged onto a monochromator with any of the detectors mentioned above.

Laser ablation is the only technology that offers direct solid sampling from *any* material and *without* sample preparation. Sampling is initiated by optical absorption processes, thereby eliminating all restrictions on sample type, size, or geometry. Elimination of sample preparation is important, especially for hazardous materials. Another unique feature is that the sampling area is micrometers in diameter, so that spatial analysis is possible. With these advantages, why is laser ablation not used more widely—are there no problems? Of course there are! The explosive laser material interaction is not fundamentally defined; it cannot

easily be predicted or controlled. For unknown samples, it is impossible to know, *a priori*, how much sample will be ablated, or whether the laser-

sampled material will be a stoichiometric representation of the solid. The quality of ablated sample and its composition depend on the laser and

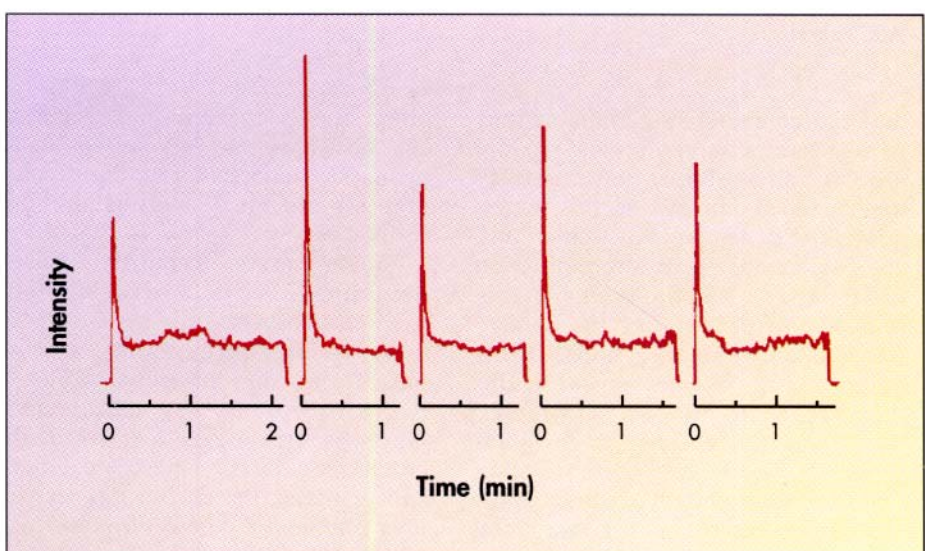


**FIG. 6. Ni emission time response from the ICP during repetitive pulsed laser ablation of steel at five separate locations on a stainless steel surface; 8-ns pulses from a 10-Hz Nd:YAG laser.**

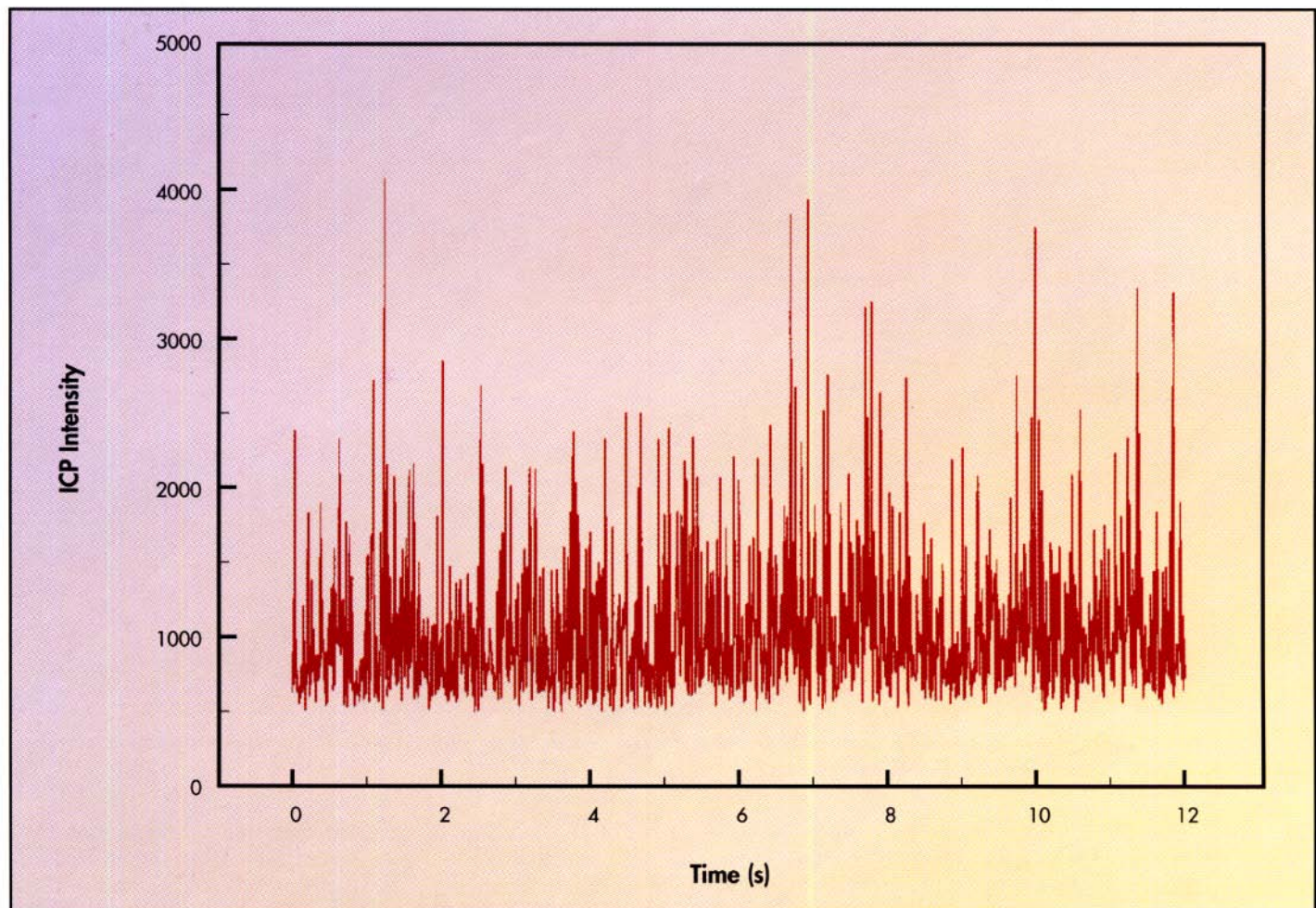


**FIG. 7.** Cu emission time response from the ICP during repetitive laser ablation of copper at  $0.1 \text{ GW/cm}^2$ . Spikes in intensity are observed on a continuous Cu emission background. Obtained with a 100-ps rise-time photomultiplier tube detector with a 500-Hz ADC rate.

material characteristics. Fluctuations in the laser's temporal and spatial profiles and nonlinear power density dependence contribute to this uncertainty. The sample's physical and chemical matrix will affect ablation behavior, and variations in the particle-size distribution of the ablated material will influence transport efficiency to the excitation source. But these problems are not show-stoppers, only concerns. Significant progress already has been made in understanding and using laser sampling technology, and commercial devices already exist for coupling to ICP sources. The issue is, How can we overcome these remaining concerns and better utilize laser sam-

pling for controlled and accurate chemical analysis? Several advancements in understanding laser ablation for chemical analysis are described below.

**Single versus Repetitive Laser Sampling.** Most laser sampling studies employ high-powered, single-pulse lasers. Because the laser is pulsed, the emission signal from the ICP will be transient, with a temporal profile characteristic of the chamber volume, the transport tube length and diameter, the carrier gas and its flow rate, and the detection electronics. For spatially resolved analysis of inhomogeneous samples, only a single laser pulse is preferred, and the temporal emission signal can be re-

solved. Unfortunately, the history of laser sampling is plagued by poor accuracy and precision for single-pulse sampling (30–70% RSD).<sup>4–6</sup> Single-pulse sampling is like bomb testing; you have only one shot to accumulate data about an explosion!

For homogeneous samples (and inhomogeneous samples when either an internal standard or external monitor is used—to be discussed later), a repetitively pulsed laser allows the sampled material from successive ablations to mix, providing *continuous* and/or *constant* ICP-AES signal response. An example of continuous and constant response is shown in Fig. 6 for Ni emission ( $\lambda = 352 \text{ nm}$ ) intensity in the ICP at five separate

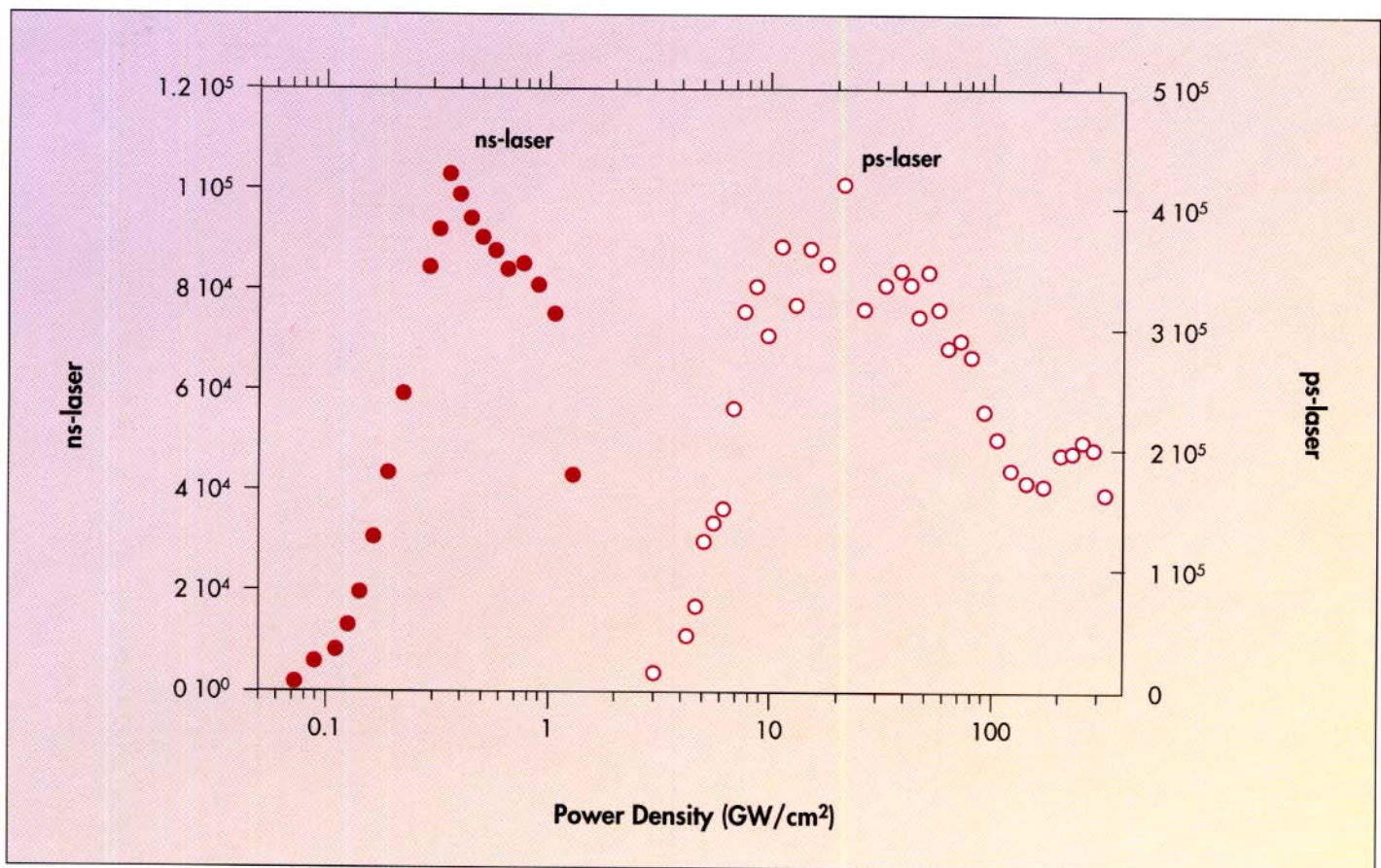


FIG. 8. ICP-AES from Cu with a picosecond Nd:YAG laser ( $\lambda = 266$  nm, energy = 6 mJ) and a nanosecond excimer laser ( $\lambda = 248$  nm, energy = 30 mJ). Each power density data point was measured during continuous emission.

locations on a steel surface.<sup>15</sup> Each temporal profile represents the emission intensity during repetitive laser sampling at a different spot on the sample, with the use of the third harmonic ( $\lambda = 365$  nm) of a Nd:YAG laser (pulse width = 8 ns) with a power density of 0.6 GW/cm<sup>2</sup>. The repetition rate was 10 Hz. The temporal behavior is dependent on the focal length of the lens, power density, etch rate of the material, and aspect ratio of the induced crater. The initial response is usually irreproducible as shown, after which time the intensity drops initially but then remains at a level that is essentially constant. The constant signal provides excellent reproducibility (RSD = 4.3%) compared with that of the maximum peak response (RSD = 25.6%) for the five measurements. The 4.3% RSD could be improved

by using lasers with better spatial and temporal properties. The nanosecond Nd:YAG laser exhibits random mode spikes on its temporal profile. Injection seeding of this laser may provide an additional improvement in laser sampling precision.

Compared to a single-pulse interaction, continuous or constant response provides better reproducibility for analysis, and a unique "controlled" environment for studying laser ablation mechanisms.<sup>15,16</sup> In the remainder of this paper, ICP-AES data are reported only when the temporal intensity behavior is approximately constant during repetitive laser sampling. For every sample we have studied, continuous emission intensity can be obtained, although it is not always constant. Several capabilities beneficial to chemical analysis are immediately recognized

from the improved precision. Optimization of the ICP for direct introduction of solids is possible during constant sampling. The power level to the ICP, gas flow rates, and detection height can be varied to obtain the best signal-to-noise (S/N) and signal-to-background (S/B) ratios. Atom-formation processes in the ICP will be different during laser sampling than they are in liquid nebulization, and can be studied. Importantly, the excellent precision allows studies of ablation mechanisms as a function of laser properties, materials, and gas environments.

#### LASER ABLATION STUDIES DURING CONTINUOUS EMISSION

**"Spikes".** In addition to atoms, ions, and molecules, laser sampling

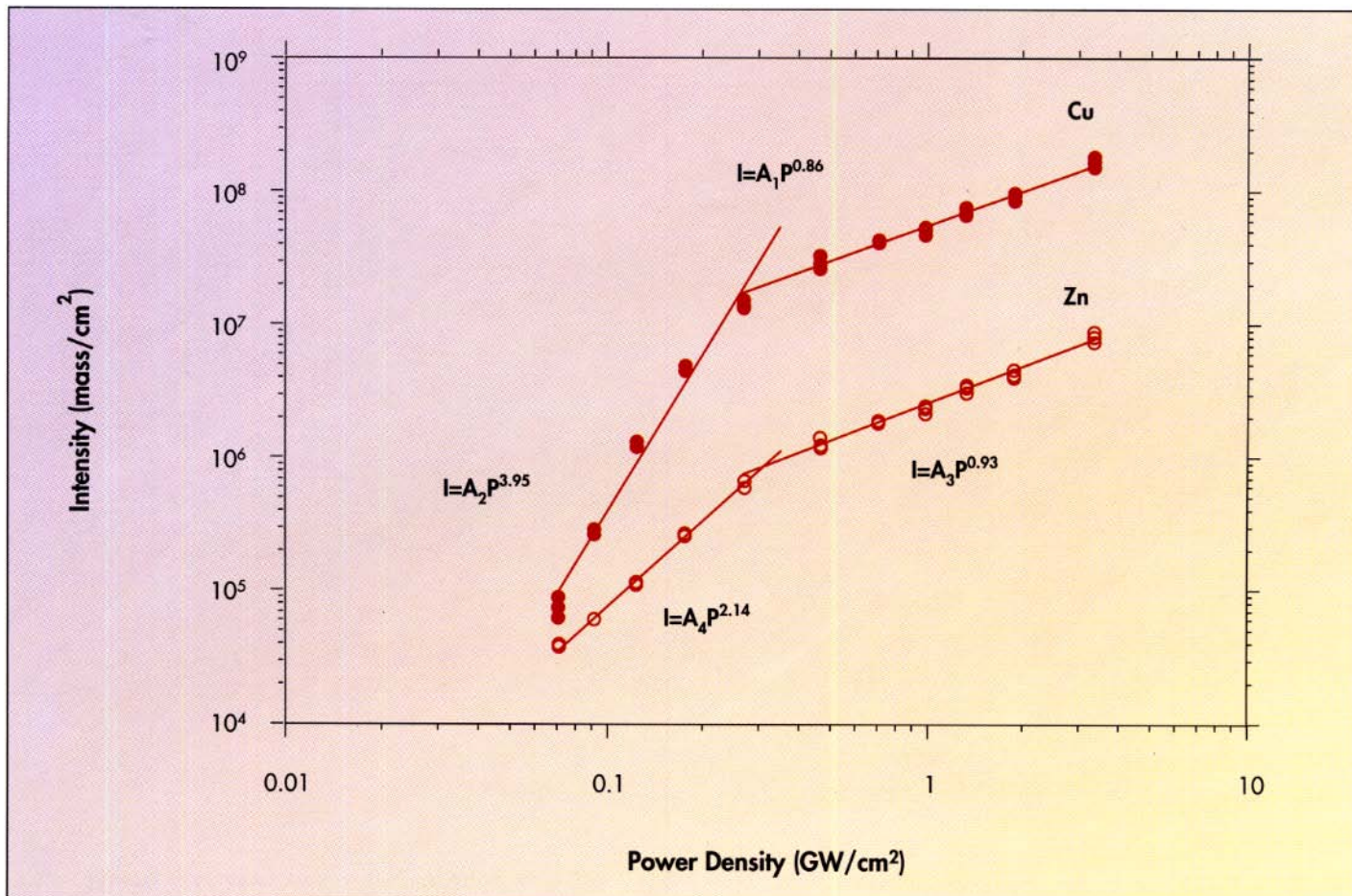


FIG. 9. Mass ablation rate behavior measured with the use of ICP-AES during nanosecond laser ablation of brass;  $\lambda = 248$  nm. Data show different rate behavior for Zn and Cu at power densities above and below approximately  $0.3\text{ GW}/\text{cm}^2$ . This change suggests a difference in ablation mechanism.

generates particles. The particle-size distribution depends on the sample material and power density of the laser beam. Sample entrainment into the carrier gas is particle-size dependent, with the majority of the particles larger than  $2\text{ }\mu\text{m}$  left behind because of low transport efficiency.<sup>17,18</sup> The measured constant signal intensity is primarily from the ensemble of “smaller” particles. However, some large particles will be entrained, and they can be observed as positive “spikes” on the emission signal if the detection electronics and data acquisition are fast enough.<sup>19</sup> Figure 7 shows the emission from spikes that results when a monochromator with a fast PMT detector measures Cu emission ( $\lambda = 324$  nm) from the ICP during laser sampling

of copper. The excimer laser ( $\lambda = 248$  nm, pulse width = 20 ns) was used at a 10-Hz repetition rate. The power density was  $0.1\text{ GW}/\text{cm}^2$ . A continuous signal intensity is obtained, with large excursions caused by individual larger particles. The emission spikes are due to Cu emission at 324 nm as the particle vaporizes and atomizes, and are not due to incandescence. The large number of spikes measured here is a worst-case scenario; the low  $0.1\text{ GW}/\text{cm}^2$  power density is known to cause substantial melting and ejection of molten droplets. The number of particles is reduced as the power density is increased. The spike-intensity will be “averaged” into the baseline if a detector with long integration time is employed, as was

the case for the data in Fig. 6. Fundamentally, it may be possible to correlate emission intensity of the spikes to particle-size distribution—important knowledge for understanding laser ablation mechanisms.

*Roll-Off.* Continuous atomic emission from the ICP provides the necessary precision to accurately measure changes in the quantity and composition of the laser-sampled vapor. For increased sensitivity, the laser power density can be changed to increase the quantity of sample delivered to the ICP. However, the efficiency of laser-energy coupling to the sample changes with power density, as demonstrated by ICP-AES measurements for both picosecond and nanosecond repetitive laser sampling (Fig. 8).<sup>7,9,20</sup> These data are for

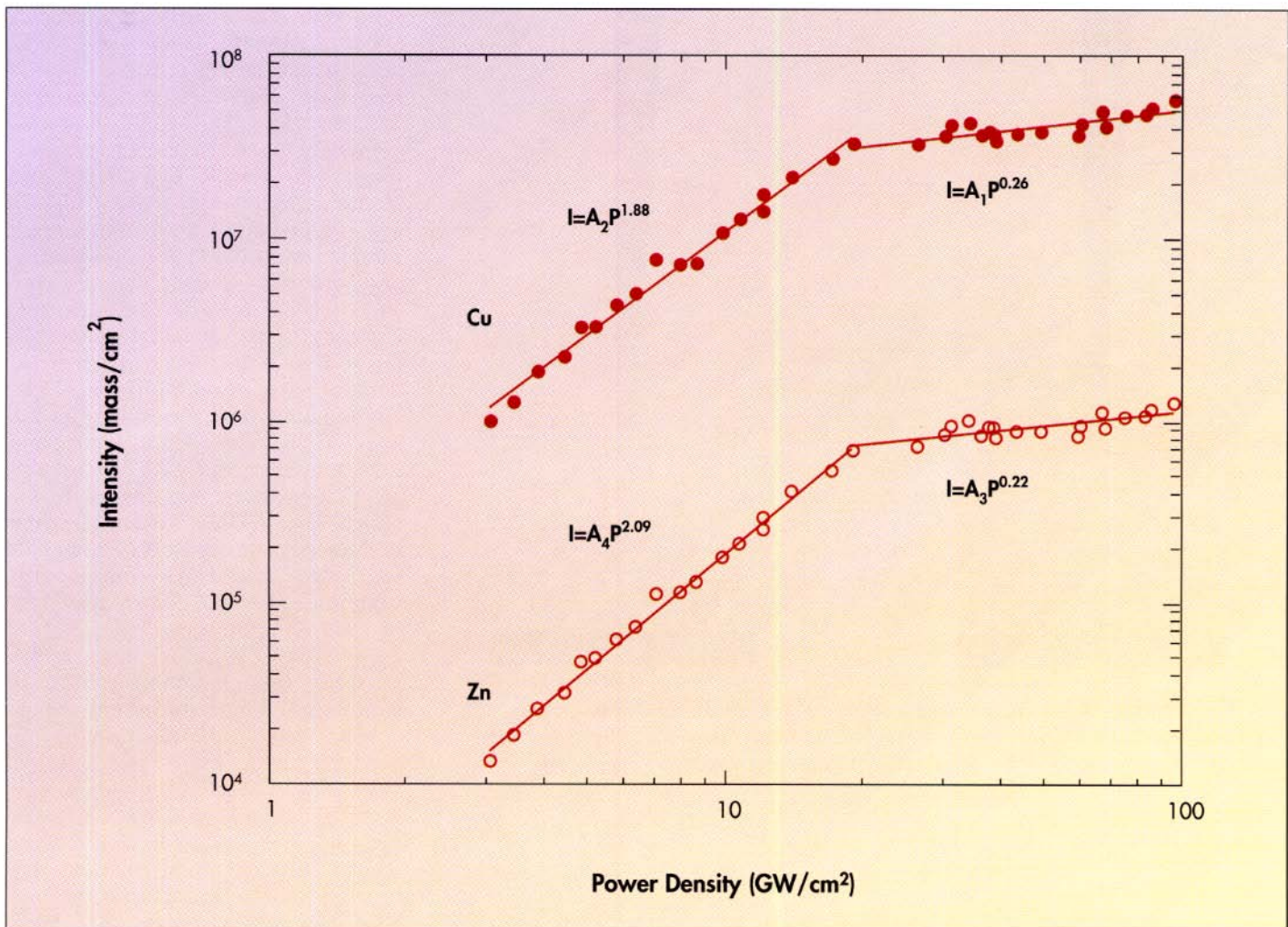


FIG. 10. Mass ablation rate behavior measured with the use of ICP-AES during picosecond laser ablation of brass;  $\lambda = 266$  nm. Data show similar rate behavior for Zn/Cu as did those for the nanosecond laser (cf. Fig 9).

Cu emission during laser sampling of pure copper samples (pure materials are used for demonstration). Each data point was measured after constant response was obtained during repetitive laser pulsing (cf. Fig. 6). ICP-AES changes reflect changes in the laser–material interaction (assuming at this point that sample transport is not affected). Several important observations from these data are that (1) the picosecond laser is more efficient than the nanosecond laser for removing sample, and (2) the sample quantity (ICP-AES intensity) exhibits a strange power density dependence. The lower-energy (6-mJ) picosecond laser ( $\lambda = 266$  nm) provides higher ICP-AES intensity

than the higher-energy (30-mJ) nanosecond laser ( $\lambda = 248$  nm), pointing out the importance of the energy deposition per unit time. For both lasers, the quantity of material increases with power density, but only up to a certain power density, at which point the quantity goes down. The plateau in intensity and roll-off (decrease) are not due to sample loading or optical self-absorption in the ICP. Instead, the roll-off is due to a change in the efficiency of laser energy coupling to the target by increased absorption and/or reflection from the laser-induced plasma, a process known as plasma shielding (to be discussed below). Similar behavior was observed for numerous

samples, including metals, alloys, oxide insulators, and glasses.<sup>19–22</sup> The roll-off occurs for all materials, for both picosecond and nanosecond sampling. An interesting observation is that the roll-off is usually measured at about 0.2–0.3 GW/cm<sup>2</sup> for conducting materials as well as for some insulators, when UV nanosecond laser pulses (and Ar as the carrier gas) are used.

In these experiments, the spot size of the laser beam was reduced in order to increase the power density. Mass ablation rate is defined as the total mass ablated per unit time and unit area. Therefore, emission intensity divided by laser beam area is proportional to mass ablation rate.

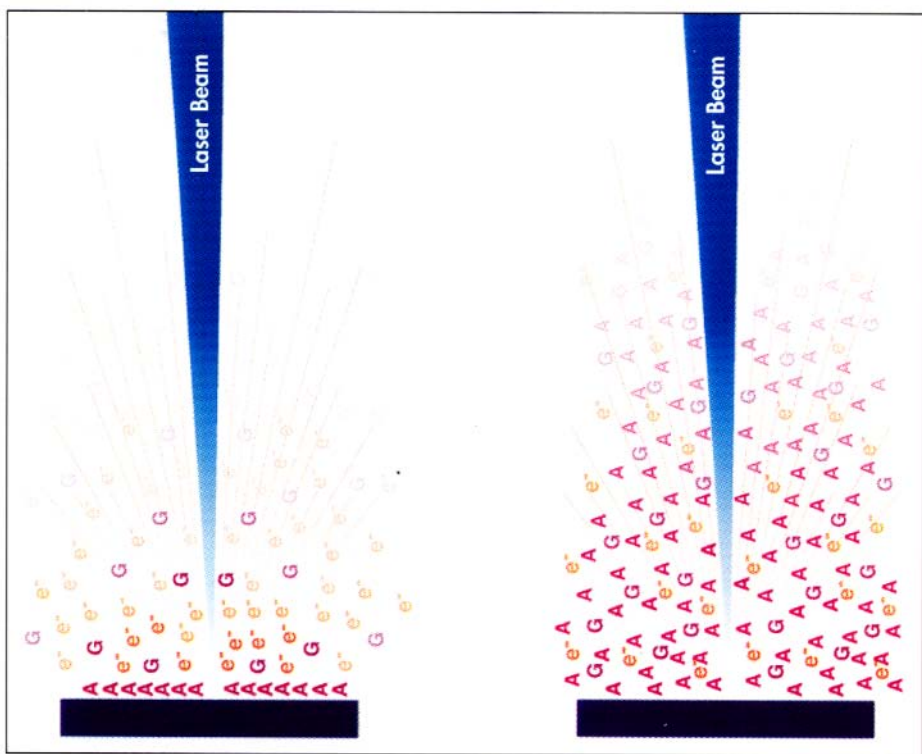


**FIG. 11. Conceptual models for plasma shielding. (Left)** Picosecond laser plasma shielding based on collisions between fast electrons and gas atoms. **(Right)** Nanosecond laser plasma shielding based on collisions between vaporized atoms/ions.

The mass ablation rates for Zn and Cu (brass sample) vs. power density are shown in Figs. 9 and 10, with nanosecond and picosecond laser sampling, respectively (the same laser conditions as above were used for these measurements).<sup>23</sup> Brass is an excellent sample to employ in these studies. The brass sample contains 60% copper (bp, 2567 K) and 40% zinc (bp, 907 K). The rates follow a power law dependence with two distinct slopes over this laser power density region. The mass ablation rate increases exponentially in the low power density regime and drops to near unity, or less, at high power densities. The mechanisms governing this power law dependence are under investigation. For the UV nanosecond sampling, Zn and Cu exhibit different mass ablation rates with power density before the roll-off. Unfortunately, this difference means that the ratio of Zn to Cu varies as a function of power density. The rates and ratios become

essentially constant after the roll-off. For the picosecond case, the rates and the ratios are essentially the same in both regions. What mechanism is responsible for the fractionation in the nanosecond case? Is the thermal component of the interaction significant in the lower power density range? If plasma heating were dominant, the rates would be expected to deviate at higher power density. A preliminary thermal-based model with inverse *bremsstrahlung* plasma absorption predicts the vaporization rate change and roll-off behavior.<sup>24</sup>

#### LASER-INDUCED PLASMAS AND PLASMA SHIELDING

The laser-induced plasma itself was hypothesized earlier as the culprit responsible for reducing the efficiency of laser sampling at elevated power density. Several studies have been performed to test this hypothesis. The initiation of a plasma at the

sample surface and its characteristics (electron density, temperature, temporal behavior) are governed by the laser beam properties (pulse duration and wavelength), by the material composition, and by the gas environment. The plasma is initiated and sustained by inverse *bremsstrahlung* absorption during collisions among sampled atoms and ions, electrons, and the gas species.<sup>25–27</sup> Plasma shielding can be studied by measuring mass ablation rate behavior in the ICP as a function of laser pulse duration and wavelength, and gas environment. The atmosphere in the ablation chamber (which is also the ICP sample carrier gas) can be any of the inert gases. As long as the total gas composition is constant, the ICP temperature and excitation characteristics should be constant for studying effects of gas environment on laser ablation sampling.

Ar is easier to ionize than He because of its higher ionization cross section and lower ionization potential; as a result, plasma shielding is expected to be more severe in Ar than in He. Plasma shielding can best be demonstrated by using the 1064-nm wavelength from the picosecond Nd:YAG laser, since inverse *bremsstrahlung* is proportional to the laser wavelength squared ( $\lambda^2$ ). With this longer wavelength, Cu emission intensity was 16 times higher with He than it was with Ar in the ablation chamber.<sup>21</sup> In support of the enhanced ICP-AES data, crater volumes were measured to be greater in the He atmosphere. (Note: a direct correlation of crater volume to changes in ICP-AES measurements is impossible; see Figs. 2 and 3). Nevertheless, a larger crater produced with the He atmosphere supports a reduced plasma-shielding mechanism and enhanced laser energy coupling to the target. With the picosecond laser at 266 nm, the enhancement in ICP-AES intensity was only a factor of 3.3 in He in comparison to that in Ar. This wavelength dependence supports the inverse *bremsstrahlung* mechanism. For the excimer laser with 20 ns pulses and  $\lambda = 248$  nm, the gas at-

mosphere had a smaller influence on ICP-AES signal levels. The Cu emission intensity was only 1.3 times higher in He than in Ar, in contrast to the behavior with the picosecond laser ( $\lambda = 266$  nm). This different influence of gas atmosphere is due to the laser pulse duration, since the photon energy is essentially the same.

The difference is plasma shielding for picosecond and nanosecond laser ablation can be explained on the basis of collisions among atoms, ions, and electrons in the atmosphere above the target surface (Fig. 11). During the picosecond laser pulse, ejected atoms/ions travel only a few hundred Ångstroms from the surface, assuming velocities on the order of  $10^6$  cm/s.<sup>28</sup> In contrast, high-energy ( $>100$  eV) electrons are generated during picosecond interactions, and these electrons can acquire velocities on the order of  $10^9$  cm/s. These fast electrons travel several hundred micrometers during the laser pulse duration, and undergo many more collisions with the gas atoms than the ejected atoms or ions.<sup>29</sup> The fast electrons absorb laser photons during collisions with the support gas atoms (Fig. 11, left). Ar and He at pressures ranging from  $10^{-5}$  Torr to 1 atmosphere were used to demonstrate plasma shielding based on an inverse *bremsstrahlung* model involving fast electrons and the support gas atoms.<sup>21</sup> The model predictions exhibited good agreement with measured changes of the crater depth with gas pressure (Fig. 12). As pressure increases, the number of electrons (ionization) increases; the laser energy incident on the sample and available for removing material is correspondingly reduced.

During the nanosecond laser pulse, the distance that atoms and ions travel from the sample surface is several hundred micrometers (Fig. 11, right). (Fast photoelectrons have not been observed for nanosecond laser ablation.) The sample atoms/ions undergo collisions with each other as they expand into the gas, and absorb photons from the laser beam (inverse *bremsstrahlung*). For

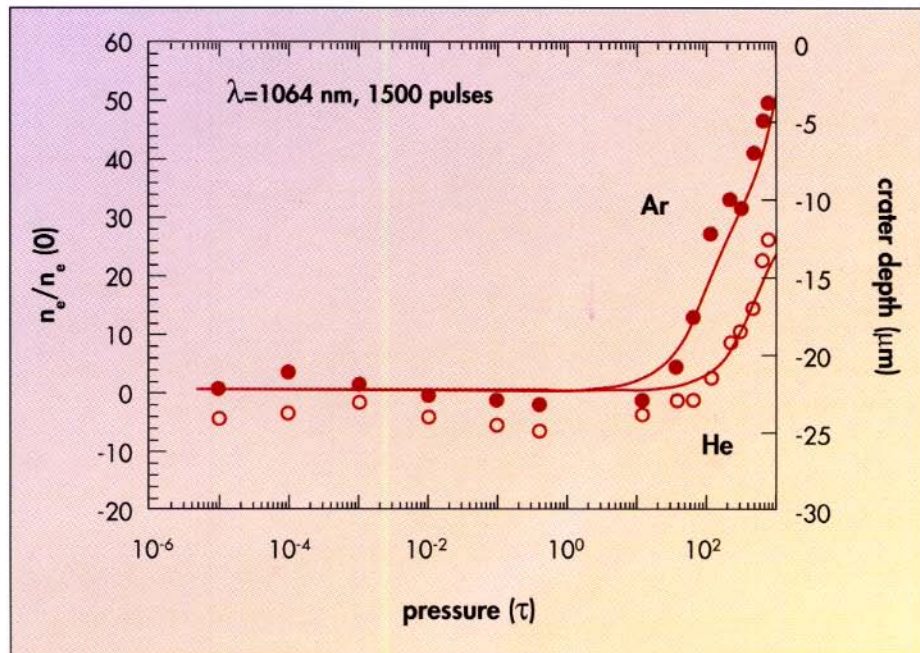


FIG. 12. Experimental change in the crater depth (data points; right axis) vs. pressure for Ar and He. Solid curves (left axis) calculated from model based on inverse bremsstrahlung for change in number of electrons (ionization) in the plasma.

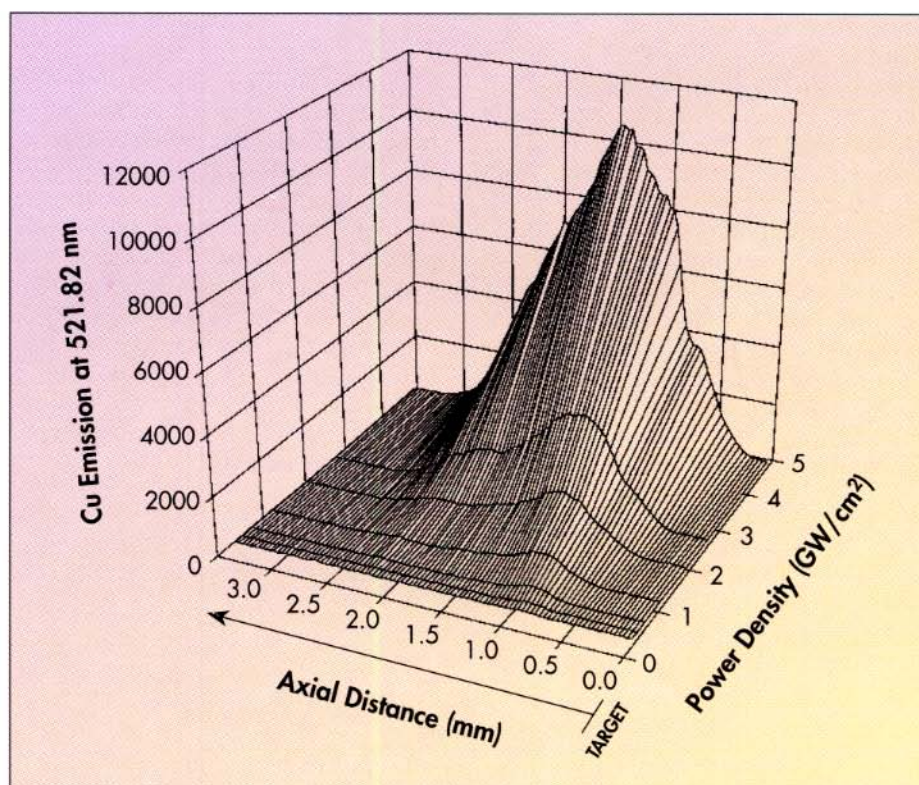


FIG. 13. Spatial distribution of the Cu(II) 521.82-nm emission intensity as a function of laser beam power density. Nanosecond excimer laser;  $\lambda = 248$  nm.

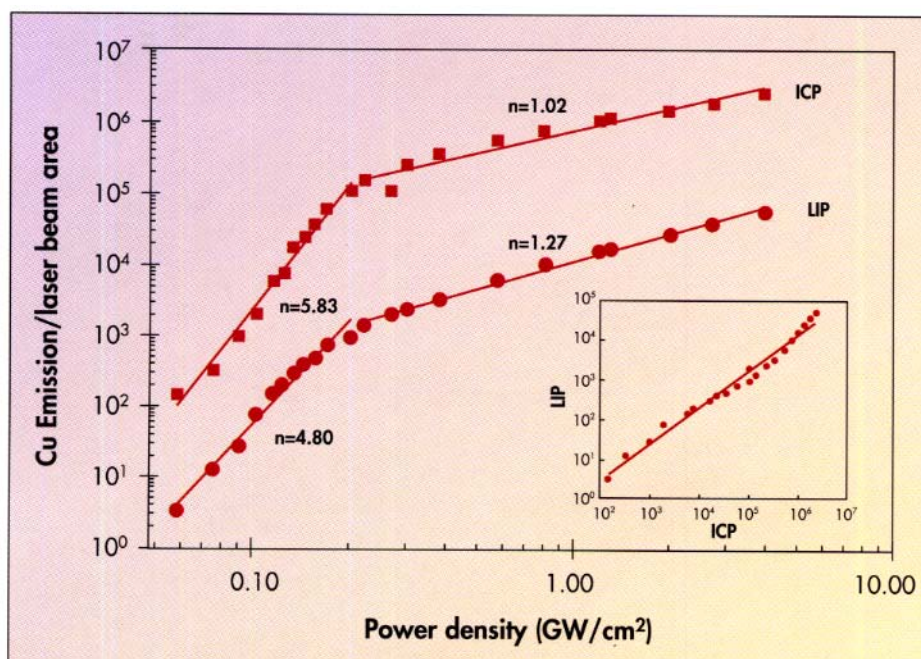


FIG. 14. Mass ablation rate (Cu emission intensity normalized to laser beam area dependence on power density for the ICP and LIP). The inset shows the correlation of the two curves.

laser ablation of copper, the plasma will be composed mainly of copper atoms and ions (instead of Ar or He ions). The ionization potential of copper (7.724 eV) is significantly lower than that of Ar and He. The photon energy of the excimer laser is 5.0 eV; only two photons are needed for multiphoton ionization of the Cu atoms, compared to four and five for Ar and He, respectively. The Cu plasma is established during the nanosecond laser pulse on the basis of these atom/ion collisions and multiphoton absorption. Collisions of gas species with the ejected atoms and ions are negligible during the nano-

second laser pulse. Therefore, the gas environment influence is not significant.

Understanding plasma initiation and reducing plasma shielding is beneficial to the use of laser ablation for chemical analysis. Improved sampling efficiency as a function of laser power density can provide increased sensitivity in chemical analysis. On the basis of the above ICP-AES data, ultraviolet wavelengths are better than those in the infrared, and a picosecond pulse duration is better than is a nanosecond. Following this trend, X-ray femtosecond pulses may be even better!

## CORRELATION OF SPECTRAL EMISSION INTENSITY IN THE ICP AND LIP

The laser-induced plasma itself can be used as a monitor to verify that the ICP-AES intensity behavior is related to ablation processes, and not to sample transport. Measuring and interpreting spatial and time-dependent emission intensity from these plasmas can be complicated.<sup>30</sup> Spatial emission intensity is a function of power density as shown in Fig. 13. However, by measuring LIP emission intensity with a long integration time and over the plasma's entire spatial extent at each power density, one can determine mass ablation rate behavior.<sup>31</sup> The LIP emission intensity shows a linear relationship with laser power density, but with distinct regions, just as did the mass ablation rate measurements described earlier (cf. Figs. 9 and 10). The data in Fig. 14 show the LIP-AES and ICP-AES behavior during laser ablation of copper. The inset in the figure shows the correlation between the LIP-AES and the ICP-AES response over this same power density range. Similar data were obtained for brass, aluminum, iron, steel, zinc, aluminum oxide, iron oxide, and glass. The good correlation was obtained for all the samples except zinc, which may be due to the low melting point of this metal. The correlation of ICP to LIP emission was observed in two cases, when only the central channel of the LIP or the entire LIP was imaged by the spectrometer. The correlation with LIP demonstrates that the ICP accurately reflects changes in laser ablation, and that transport does not influence these data.

## LASER ABLATION ICP-AES OF GLASS (AN ANALYTICAL STUDY)

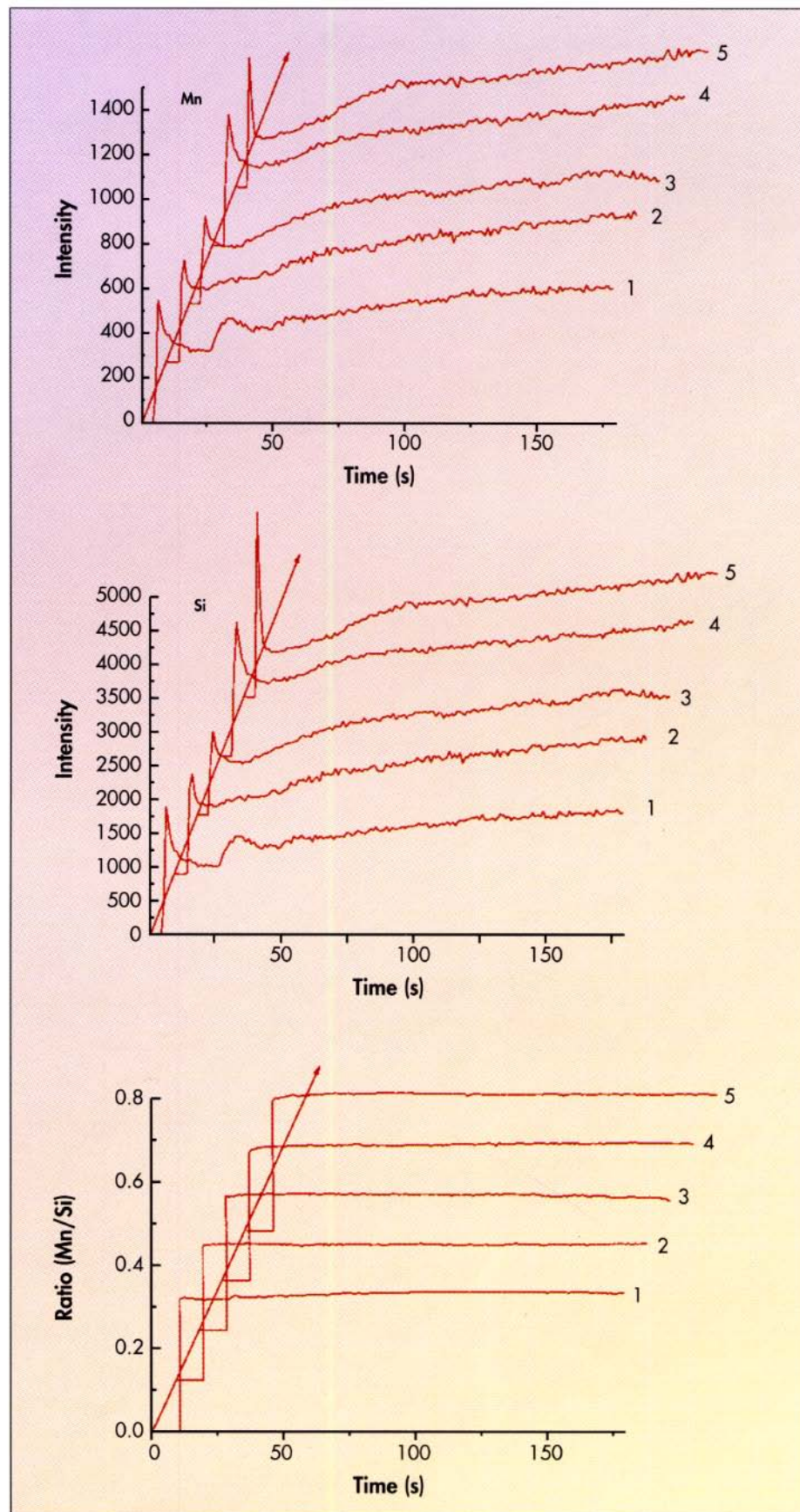
UV laser ablation sampling with ICP-AES was applied to the elemental analysis of prototypic vitrified waste glass samples from the Savannah River Technology Center.<sup>22</sup> Laser ablation sampling has been proposed as an excellent alternative to

TABLE II. Emission intensity ratios to Si and the precision for the major elements from an SRTC prototypic glass.

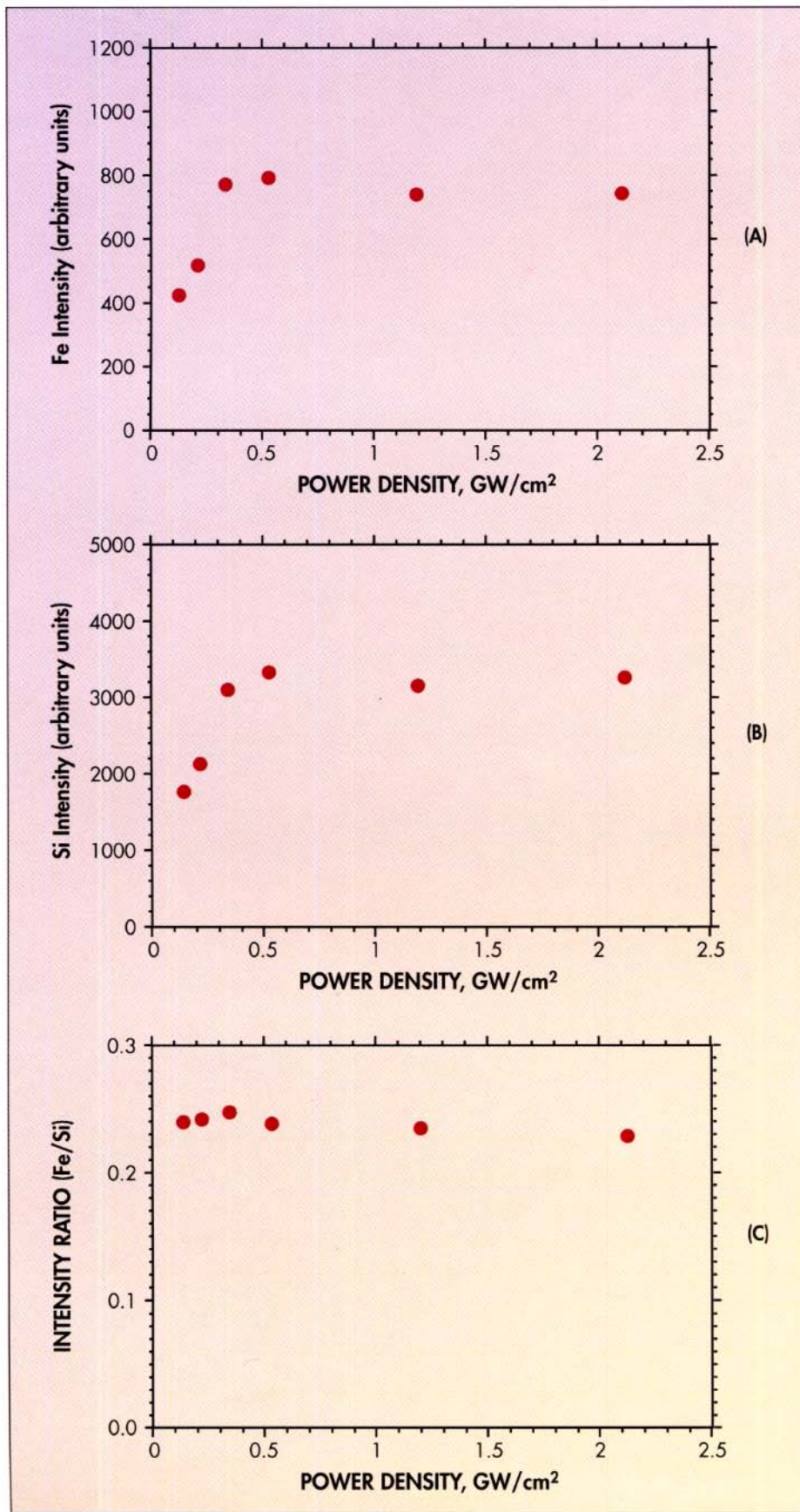
Oxide	Composition (%)	Avg. spectroscopic intensity ratio (5 spots)	Standard deviation	Relative standard deviation (%)
MnO <sub>2</sub>	2.11	0.3279	0.0010	0.31
Fe <sub>2</sub> O <sub>3</sub>	12.80	0.2676	0.0011	0.42
MgO	1.42	2.4360	0.0181	0.74
Al <sub>2</sub> O <sub>3</sub>	4.88	0.4176	0.0065	1.56

dissolution procedures when vitrified waste products that may be highly radioactive are being dealt with. Five major elements in the prototypic glass samples were selected for analysis (Table II). These elements were chosen to provide good signal-to-background ratios simultaneously with the use of the PDA spectrometer, which is not a particularly sensitive instrument.

The data in Figs. 15a (top) and 15b (middle) show the temporal behavior of ICP-AES emission measured for Mn and Si, with the use of, for ablation, the nanosecond-pulsed excimer laser ( $\lambda = 248$  nm) with a power density equal to  $1.2 \text{ GW/cm}^2$  at a repetition rate of 10 Hz. At this power density, fluctuations in laser power are linearly related to those in the signal. The curves in Figs. 15a and 15b show the sample removal time response from Mn and Si during repetitive (continuous) ablation at five different locations on a shard of prototypic glass. As expected, the response was continuous although not constant, because of fast etching rates for these samples. For each spot, the signal from the first one hundred pulses (the initial peak in the profiles) varies significantly (up to 50% RSD). The precision for the five spots after 60 s of pulsing improves to 5–8% RSD, consistent with the power fluctuations of the laser. The temporal profile of emission for the elements in Table II exhibited similar behavior. Si was chosen as an internal standard, and the intensity ratio to Si for the other four elements was measured to be constant both in time and between spots, except for the first 10 s [Fig. 15c (bottom)]. The intensity ratios have excellent precision; for the five craters, the RSD varied from 0.3 to 1.7% (Table II).



→  
Fig. 15. Time-dependent ICP-AES intensity during repetitive (10-Hz) nanosecond excimer ( $\lambda = 248$  nm) laser ablation of SRTC prototypic glass. Power density =  $1.2 \text{ GW/cm}^2$ . (Top) Mn; (middle) Si; (bottom) Mn/Si ratio. Each time trace is a separate spot on the glass.



The constant ratios demonstrate that there is no time-dependent fractionation of these elements, at this power density. Also, these data demonstrate that the glasses are homogeneous in elemental composition throughout the crater depth. The crater diameters are about 200  $\mu\text{m}$  and the depth is on the order of 1000  $\mu\text{m}$  after 900 laser pulses. The sampling rate is, therefore,  $\sim 1 \mu\text{m}$  per laser shot. Depth profiling with this resolution or better is therefore possible.

With a fixed laser beam energy and translation of the focusing lens to obtain spot sizes from approximately 1000 to 200  $\mu\text{m}$ , the power density was varied from 0.13 to 2.12 GW/cm<sup>2</sup>. The ablated quantity of glass sample increased with the power density and reached a maximum at  $\sim 0.3 \text{ GW/cm}^2$  (Fig. 16). The plateau in intensity due to plasma shielding is evident (these data are not normalized to area). Figures 16a (top) and 16b (middle) show the data for Fe and Si as a function of power density, respectively. Each data point in these graphs represents the average intensity from five spots, measured during *continuous* emission. Relative to that for Si, the intensity ratio for Fe remains essentially constant over this power density range [Fig. 16c (bottom)]. Similar behavior was measured for Mg, Al, and Mn. Therefore, the irregular surface of a glass shard and thus slight variation in lens-to-sample distance did not influence the mass ablation behavior. The fact that the ratio remains constant for these elements indicates that preferential vaporization of these elements also is not significantly influenced by power density, over this range.

Seven SRTC prototypic glass samples were available, with slightly varied oxide concentrations. A quan-

FIG. 16. ICP-AES signal vs. laser power density with the use of excimer laser ablation. Each data point represents the average of five spots, measured once continuous sampling was obtained.

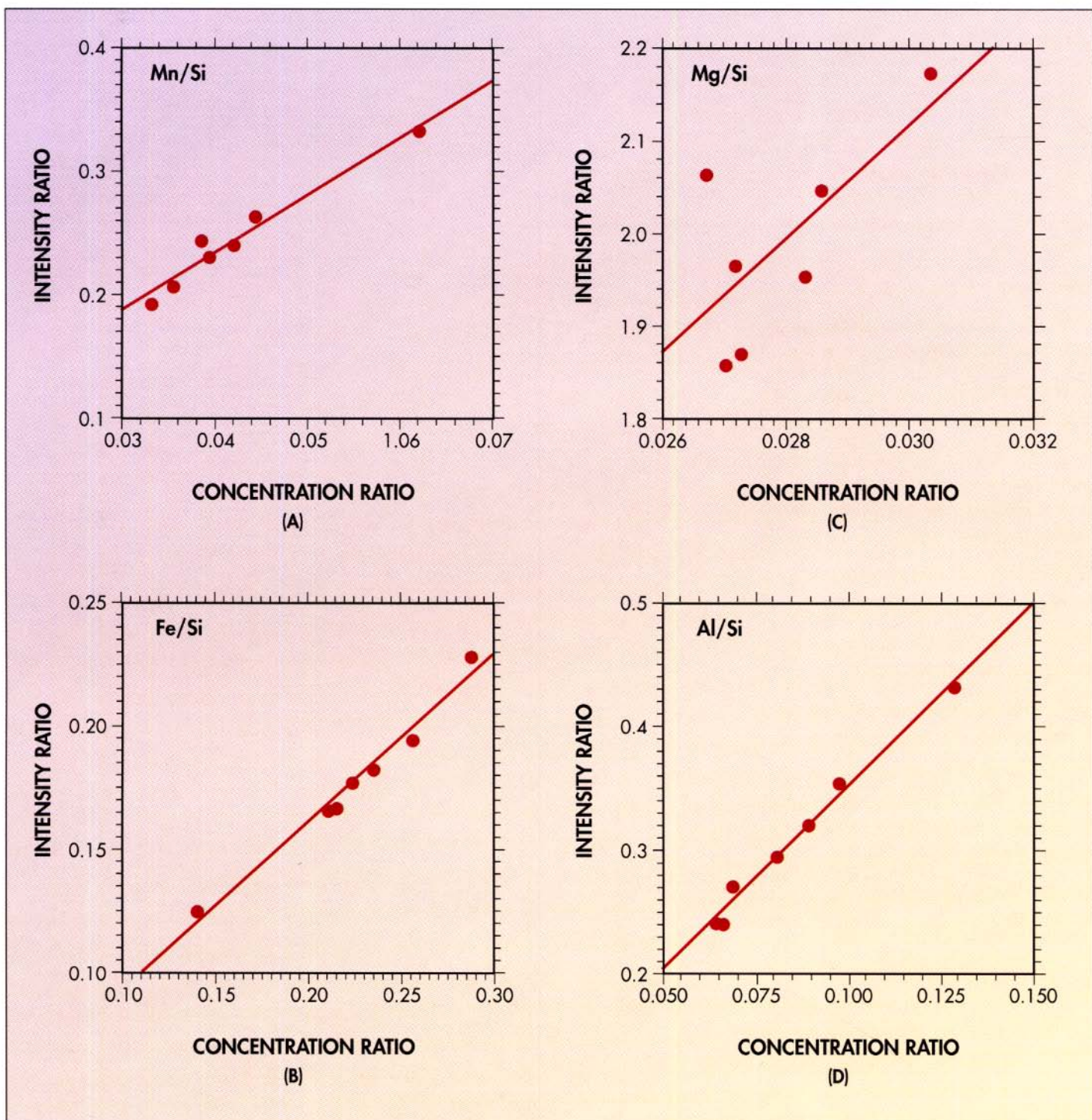


FIG. 17. Calibration curves for measured elemental:Si ratios vs. the prepared (nominal) composition. Nanosecond excimer laser sampling of SRTC prototypic glass with ICP-AES was employed.

titative study showed linear calibration curves when Si was used as the internal standard (Fig. 17). The ordinate is the measured emission intensities, ratioed to Si, and the ab-

scissa is the prepared oxide concentration ratios. The correlation coefficients for these data are 0.98 to 0.99, except for that of Mg, which is 0.70.

## THE FUTURE

This intentionally *brief* discussion turned out to be long, and laser ablation has barely been addressed!

**TABLE III.** "Ideal" laser sampling characteristics for chemical analysis.

- Laser absorbed linearly with energy and power
- No interaction of laser with ambient medium
- Heat-affected zone = optical penetration depth
- No melting or fractionation
- No interaction of vapor plume with ambient gases
- Narrow particle size distribution
- 100% transport efficiency
- Fixed concentration of an element in *any* matrix gives the same ICP-AES intensity

Where do we go from here? Laser ablation is here to stay. It has found a niche in numerous applications, extending far beyond the analytical realm, into areas of fusion energy, medicine, materials, materials processing, and a new exciting field, pulsed laser deposition (PLD). For PLD, any material can be "sampled" and the vapor deposited as a thin film. The new high-temperature superconducting (HTSC) materials have provided an "explosion" of laser ablation technology.<sup>32-36</sup> In the words of Richard L. Gordon, "laser ablation applications are outpacing fundamental understandings".<sup>37</sup> The same issues influencing laser ablation for chemical analysis hold for these other applications. One thing is clear, though: analytical spectroscopy is an important technology for elucidating laser ablation behavior. Through these and related studies, laser ablation can evolve from an uncontrolled and unpredictable explosion to one that is routinely used for analytical chemical analysis. Table III summarizes ideal conditions we endeavor to achieve.

## ACKNOWLEDGMENTS

This paper would not be possible without excellent discussions, and experimental and theoretical contributions, from Xianglei Mao, Mark Shannon, Wing-Tat Chan, Alberto Fernandez, Manuel Caetano, and Marvin Kilgo. This research was supported by the U.S. Department of Energy, Office of Basic Energy Sciences, Chemical Sciences Division, Processes & Techniques Branch, under Contract No. DE-AC03-76SF00098.

1. S. A. Darke and J. F. Tyson. *J. Anal. At. Spectrom.* **8**, 145 (1993).

2. L. Moenke-Blankenburg, *Spectrochim. Acta Rev.* **15**, 1(1993).
3. L. Moenke-Blankenburg, *Laser Micro Analysis, V 105, A Series of Monographs on Analytical Chemistry and its Applications*, J. D. Wineforner and I. M. Kolthoff, Eds. (John Wiley and Sons, New York, 1989).
4. D. A. Cremers and L. J. Radziemski, in *Laser Spectroscopy and its Applications*, L. J. Radziemski, R. W. Solarz, and J. A. Paisner, Eds. (Marcel Dekker, New York, 1987), pp. 351-415.
5. K. Dittrich and R. Wennrich, *Prog. Anal. Atom. Spectrosc.* **7**, 139 (1984).
6. K. Laqua, in *Analytical Laser Spectroscopy*, N. Omenetto, Ed. (John Wiley and Sons, New York, 1979), pp. 47-118.
7. M. von Allmen, *Laser-Beam Interactions with Materials: Physical Principles and Applications* (Springer-Verlag, New York, 1987), p. 16.
8. N. Bloembergen, in *Laser Solid Interaction and Laser Processing*, S. D. Ferris, H. J. Leamy, and J. M. Poate, Eds. (American Institute of Physics, New York, 1979).
9. J. F. Ready, *Effect of High-Power Laser Radiation* (Academic Press, New York, 1971).
10. Y. V. Afanasyew, O. N. Krokin, and G. V. Sklizkov, *IEEE J. Quant. Elec.* **JQE-2**, 483 (1966).
11. J. F. Ready, *J. Appl. Phys.* **36**, 462 (1965).
12. A. A. Rostami, R. Greif, and R. E. Russo, *Int. J. Heat Mass Transfer* **35**, 2161 (1992).
13. T. J. Goldsack, J. D. Kilkenny, B. J. MacGowan, S. A. Veats, P. F. Cunningham, C. L. S. Lewis, M. H. Key, P. T. Rumsby, and W. T. Toner, *Opt. Commun.* **42**, 55 (1982).
14. W. W. Duley, *Laser Processing and Analysis of Materials* (Plenum Press, New York, 1983).
15. R. E. Russo, "Direct Solid Introduction to the ICP Using a Repetitively Pulsed Nd:YAG Laser", delivered at the Federation of Analytical Chemistry and Spectroscopy Societies Meeting, Philadelphia (1984).
16. P. Arrowsmith, *Anal. Chem.* **59**, 1437 (1987).
17. P. Arrowsmith and S. K. Hughes, *Appl. Spectrosc.* **42**, 1231 (1988).
18. M. Thompson, S. Chenery, and L. Brett, *J. Anal. At. Spectrom.* **5**, 49 (1990).
19. W. T. Chan and R. E. Russo, *Spectrochim. Acta* **46B**, 1471 (1991).
20. W. T. Chan, X. L. Mao, and R. E. Russo, *J. Appl. Spectrosc.* **46**, 1025 (1992).
21. X. L. Mao, W.-T. Chan, M. A. Shannon, and R. E. Russo, *J. Appl. Phys.* **74**, 4915 (1993).
22. R. E. Russo, W.-T. Chan, M. Bryant, and F. J. Kinard, *J. Anal. At. Spectrom.* **10**, 295 (1995).
23. W. T. Chan and R. E. Russo, "Characteristics of Laser-Material Interactions Monitored by Inductively Coupled Plasma-Atomic Emission Spectroscopy", in *Laser Ablation Mechanisms and Applications*, J. C. Miller and R. F. Haglund, Jr., Eds. (Springer-Verlag, New York, 1991), p. 53-59.
24. X. L. Mao and R. E. Russo, "Thermal Vaporization and Inverse Bremsstrahlung Model to Describe Nanosecond Plasma Shielding", deliver at the Conference on Laser Ablation (COLA), EMRS Meeting, Strasbourg, France (1995).
25. P. L. Kelley, *Phys. Rev. Lett.* **15**, 1005 (1965).
26. R. Y. Chiao, E. Garmire, and C. H. Townes, *Phys. Rev. Lett.* **13**, 479 (1964).
27. R. Fabbro, E. Fabre, F. Amiranoff, C. Garbau-Labaune, J. Virmont, M. Weinfeld, and C. E. Max, *Phys. Rev. Ser. A* **26**, 2289 (1982).
28. O. L. Landen and W. E. Alley, *Phys. Rev. A* **46**, 5089 (1992).
29. G. Farkas and C. Toth, *Phys. Rev. A* **41**, 4123 (1990).
30. X. L. Mao, M. A. Shannon, A. J. Fernandez, and R. E. Russo, *Appl. Spectrosc.* **49**, 1054 (1995).
31. A. J. Fernandez, X. L. Mao, M. A. Shannon, and R. E. Russo, *Anal. Chem.* **67**, 2444 (1995).
32. T. V. Venkatesan, in *Laser Ablation: Principles and Applications*, J. C. Miller, Ed. Springer Series in Material Science 28 (Springer, New York, 1994), pp. 313-327.
33. *Pulsed Laser Deposition of Thin Films*, D. B. Chrisey and G. K. Hubler, Eds. (John Wiley and Sons, New York, 1994).
34. R. P. Reade, P. Berdahl, L. W. Schaper, and R. E. Russo, *Appl. Phys. Lett.* **66**, 2001 (1995).
35. R. E. Russo, X. L. Mao, and D. L. Perry, *Chemtech*, December, 14 (1994).
36. R. P. Reade, P. Berdahl, S. M. Garrison, and R. E. Russo, *Appl. Phys. Lett.* **61**, 2231 (1992).
37. R. L. Gordon, Pacific Northwest Laboratories, personal communications.